SOLAR WIND IRON ISOTOPIC ABUNDANCES: RESULTS FROM SOHO/CELIAS/MTOF

F.M. Ipavich*, J.A. Paquette*, P. Bochsler†, S.E. Lasley* and P. Wurz†

*Department of Physics, University of Maryland, College Park, MD, USA 20742
†Physikalisches Institut der Universität Bern, Switzerland, CH3012

Abstract. The MTOF sensor uses time of flight measurements in a harmonic potential region to identify elements and isotopes in the solar wind with excellent mass resolution. The combination of MTOF's large bandwidth electrostatic deflection system and the 3-axis stabilized orientation of SOHO results in excellent counting statistics. We report relative abundances of the iron isotopes with mass 54, 56 and 57 amu. Since these isotopes are chemically identical, we expect little fractionation either in the solar wind or in the instrument, resulting in relatively small estimated uncertainties. Our results agree, within the measurement uncertainties, with terrestrial values.

INTRODUCTION

Observations of rare elements and isotopes in the solar wind are important because they help determine how neutral atoms in the relatively cool photosphere become the highly ionized atoms in the corona and then ultimately the supersonic plasma we call the solar wind. The results will also help establish the isotopic composition of the primordial solar nebula.

The good agreement of photospheric and meteoritic abundances [1] for a wide range of refractory and moderately volatile elements are consistent with a common origin of solar and planetary matter. The Sun is considered to contain a largely unfractionated sample of matter from the protosolar nebula; hence knowledge of solar composition can reveal the composition of the local interstellar medium some 4.6 Gy ago, and as well shed light on the chemical and isotopic evolution of planetary matter [2]. The solar wind composition is expected to be that of the solar outer convective zone, differing only as a result of possible fractionation processes. Elemental composition is subject to the well-known fractionation process ordered by the first ionization potential [3], reflecting the separation of neutrals and ions in the upper chromosphere; the magnitude of this fractionation is of order 3 or so in the slow solar wind. Isotopic composition is, however, not subject to this fractionation process; typical isotopic fractionation is expected to be at the percent level.

The Mass Time-of-Flight Spectrometer (MTOF) is one of four sensors (CTOF, MTOF, STOF, SEM) comprising the Charge, Element, Isotope Analysis System (CELIAS) Experiment [4] on the Solar Heliospheric Observatory (SOHO) spacecraft. CELIAS uses three time-of-flight (TOF) sensors to make composition measurements. MTOF has unprecedented mass resolution and collection power for solar wind composition studies, and can identify rare elements and isotopes that were previously not resolvable from more abundant neighboring species, or were not previously observable at all.

INSTRUMENTATION

The Mass Time-Of-Flight (MTOF) sensor of the CELIAS investigation is actually two subsensors. The MTOF/Main is the primary unit, providing elemental and isotopic abundance measurements of heavy ions in the solar wind. The MTOF/Proton Monitor is an auxiliary unit designed to measure the solar wind proton parameters. Both units are housed within a common structure which also contains the low voltage power converter, the high voltage power supplies, the analog electronics, and the digital electronics.

The MTOF Main Sensor

The MTOF Main Sensor (illustrated in Figure 1) is a high-mass ($M/\Delta M \approx 100$) resolution system that provides unprecedented solar wind composition data over a wide range of solar wind conditions. The high sensitivity of MTOF allows for the first time an accurate determi-

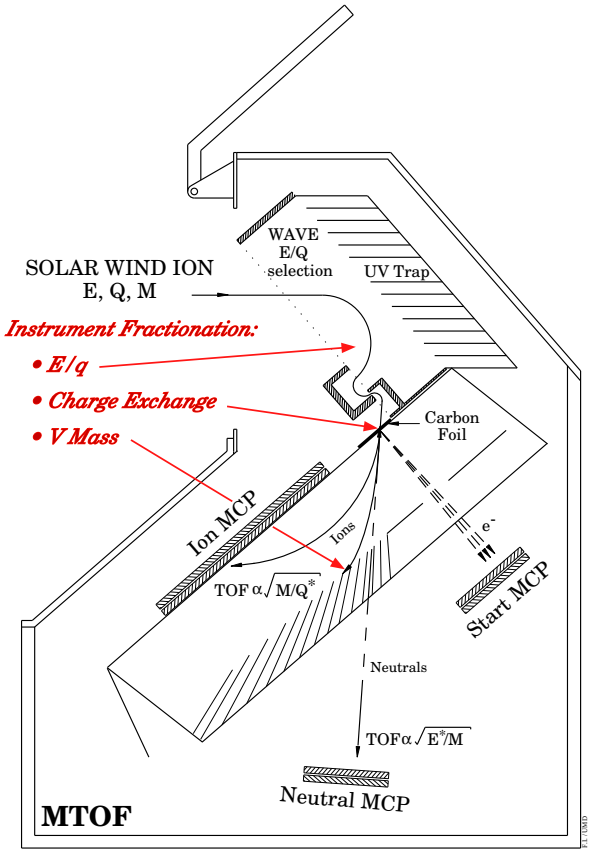

FIGURE 1. Schematic of the MTOF (Mass Time of Flight) Instrument. Solar wind ions enter through an energy/charge filter (the WAVE) and pass through a carbon foil, leaving them with a charge state q^*. They then enter a region where a special electric field bends those with $q^* > 0$ down to a microchannel plate. For an ion of mass M, the time of flight in this region is $\propto \sqrt{M/q^*}$.

nation of the abundances of many of the elements and isotopes in the solar wind. The MTOF sensor consists of the Wide-Angle, Variable Energy/charge (WAVE) passband deflection system and the time-of-flight High-Mass Resolution Spectrometer (HMRS).

MTOF owes its excellent mass resolution capability to a specially designed electric field configuration in its time-of-flight region. An ion's time-of-flight through this region is *independent* of its initial energy or angle. Sub-nanosecond TOF measurements translate into mass resolutions of a fraction of an AMU.

A prototype of the MTOF sensor, known as MASS, was flown on the WIND spacecraft (launched about a year before SOHO), and was able to identify a number of elements and isotopes for the first time. The MTOF sensor incorporates a number of enhancements over its prototype, including position-sensing and signal amplitude measurements, and improved background-rejection techniques. MTOF also generates a 2 to 3 order of magnitude improvement in counting statistics, thanks to: (a) the fact that SOHO always looks in the solar direction (unlike the spinning WIND spacecraft); and (b) a novel entrance deflection system with a very wide bandwidth (400% vs. the more typical 5% in other solar wind instruments), requiring only a few voltage steps to cover the entire energy-per-charge distribution of the solar wind. As a consequence of the very wide deflection system passband, MTOF cannot determine the charge state distribution of solar wind ions.

The MASS and MTOF sensors were designed and fabricated by the University of Maryland; their entrance deflection systems were built by the University of Bern, which also provided the primary calibration facility for these instruments.

THE MTOF TOF SYSTEM

The heart of the MTOF sensor is the time-of-flight High Mass Resolution Spectrometer (HMRS). The principal of operation of the HMRS is based on the fact that the time of flight t of an ion of mass M is proportional to $\sqrt{M/q^*}$ in the presence of an electric field that increases linearly with distance. Here q^* is the ion's charge after penetrating a thin carbon foil. Hence, the measurement of t gives unambiguous values of M/q^* for individual ions. The required electric field is produced by a combination of a hyperbolic plate set at a large positive voltage V_H (typically 20 to 25 kV) and a V-shaped plate at ground potential. The high mass resolution of the MTOF sensor is due to the fact that t is independent of the ion energy and the angle at which the ion enters the HMRS electric field. The value of V_H determines the maximum ion energy that can be deflected by the electric field, but does not affect the mass resolution. Since t can be measured with the precision of a fraction of a nanosecond, high mass resolution is achieved. Figure 2 displays a spectrum, where the TOF has been converted into mass units, near the mass range of iron.

The practical implementation of the HMRS requires an accurate measurement of t and the conversion of multiply-charged solar wind ions into singly-charged ions. This is accomplished with a combination of microchannel plate (MCP) detectors and a thin carbon foil at the entrance to the HMRS electric-field region. Ions passing through the foil undergo a large number of collisions with the carbon atoms, resulting in some energy loss, moderate scattering, and charge exchange. As a result of the charge exchange, ions with initial charge state q emerge from the foil with charge state q^*, where q^* is typically 0 or +1. As the ions leave the foil they also produce secondary electrons that are deflected to a "Start" MCP assembly that generates a start signal for the time-

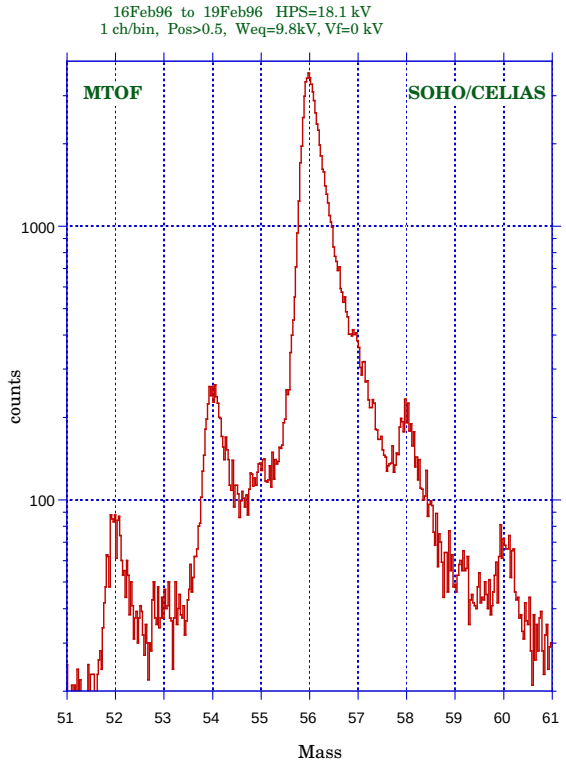

FIGURE 2. Observed solar wind mass spectrum accumulated over a 3 day period in 1996

of-flight analysis. The "stop" signal for particles with $q^* > 0$ is generated at a second large area "Ion" MCP assembly located behind the ground surface of the electric field region; for particles with $q^* = 0$, the "stop" signal is generated by the "Neutral" MCP.

The anodes for all three MCPs provide not only the required timing signals, but also amplitude signals that are pulse height-analyzed by the electronics. These amplitude signals provide some information about particle mass and energy. In addition, the Neutral and Ion MCP anodes provide 1-dimensional position information. The Neutral position is a measure of the solar wind ion's flow direction in the solar ecliptic plane, useful for interpretation of the data. The Ion position allows us to determine the E/q of an ion, and is also useful for rejecting background events.

The entire HMRS is maintained at a 'floating' voltage, V_F, in the range -5 to +5 kV. For high solar wind speeds, a positive V_F decelerates heavy ions so that they can be deflected by the hyperbola voltage and detected by the Ion MCP. For low solar wind speeds a negative V_F will accelerate the ions before they reach the carbon foil, and thereby improve the efficiency of their detection in the HMRS.

The MTOF Proton Monitor SubSensor

The MTOF Proton Monitor (PM) is designed to measure the solar wind proton bulk speed, density and thermal speed. The bulk speed (and, to a lesser extent, the thermal speed) is necessary to the evaluation of data from the main MTOF sensor. The PM is described in detail elsewhere [5].

MAXIMUM LIKELIHOOD TECHNIQUE

The counting rates in a series of Time of Flight Channels were simulated using a maximum likelihood technique. In this technique, the simulated count rate in a particular channel was taken as the mean, μ_i, of a Poisson distribution. Assuming that this Poisson distribution is the parent distribution from which the measurements were derived, the probability that any given number of counts N_i was observed in that channel is

$$P_i = \frac{\mu_i^{N_i}}{N_i!} e^{-\mu_i}$$

The probability that the measured TOF spectrum was observed, given the assumptions in the simulation, is simply the product of the probabilities for each channel:

$$P_{Tot} = \prod P_i$$

The goal of is to maximize this probability by altering the parameters of the model function, thus altering the μ_i. In practice, it is easier and equivalent to deal with the natural log of this expression:

$$\ln(P_{Tot}) = \sum_i N_i ln(\mu_i) - \mu_i - ln(N_i!)$$

A constrained minimization routine (E04KDF from the NAG Library; see [6]) was used to minimize the negative logarithm of the probability (equivalent to maximizing the positive logarithm.)

The model function used had 24 parameters. Fourteen of these were the heights of the peaks corresponding to masses 48, 49, and 52-63. Of the remaining 10, two described a linear background, two were needed to convert from mass to time of flight channel, two were associated with peaks caused by electronic "ringing" and the remaining 4 described the shape and width of the peaks. The form of the model function was a modified asymmetric Lorentzian:

$$\frac{A}{1 + ((X - X_0)/\Gamma)^n}$$

where A is the amplitude (in counts) for each of the 14 mass values, and X_0 is the peak location (in time of flight

channel number) that is derived from the mass values. The exponent, n, and the half width at half maximum, Γ, are the same for all species, but are allowed to be different on either side of the peak.

OBSERVATIONS

The mass spectrum displayed in Figure 2 was accumulated over a 3 day time period in February 1996 during which time the solar wind was of a nondescript interstream type. The maximum likelihood technique was applied to derive the abundance ratios of the Fe isotopes. These abundance ratios are then corrected by the ratios of instrument efficiencies for these isotopes. The efficiency corrections depend weakly on the solar wind speed and temperature, the deflection system and hyperbolic plate voltage settings, and the incident charge state distributions of the Fe ions, and were in the range of 1% to 4% for the time intervals selected for this paper.

The solar wind behavior during another interstream time period is shown in Figure 3. The mass spectrum accumulated during this time interval is displayed in Figure 4.

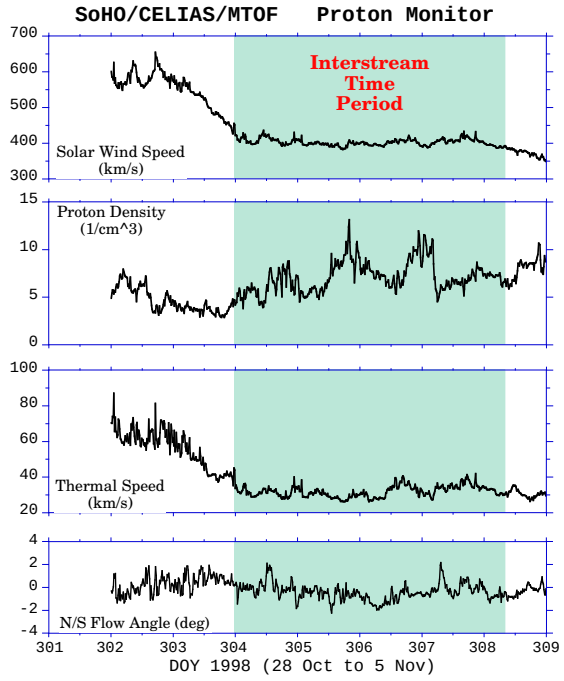

FIGURE 3. Solar wind behavior during a typical interstream time period.

In addition to the two individual time periods discussed above, mass spectra have also been obtained for two 12-month time periods (April 1996 to March 1997 and March 1997 to March 1998). For both 12-month periods, only those 5-minute intervals in which the solar wind speed was between 380 and 400 km/s were included. This was done in order to minimize the variation of the relative efficiencies.

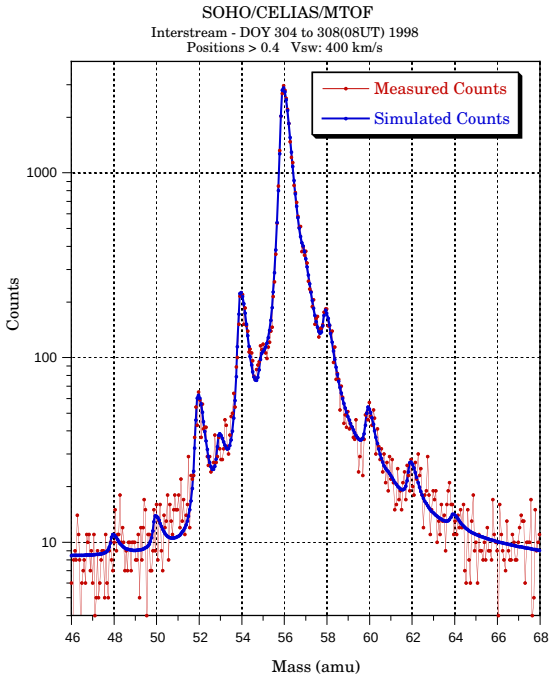

FIGURE 4. Mass spectrum accumulated during the shaded time period indicated in Figure 3. The fit from the maximum likelihood technique is indicated by the solid line.

RESULTS

The efficiency-corrected ratios derived for Fe^{54}/Fe^{56} and Fe^{57}/Fe^{56} in the 4 intervals discussed above are presented in Figure 5 and Figure 6, respectively. In each figure the terrestrial value from [7] is indicated by the solid horizontal line.

The results averaged over all 4 time periods are shown in Table 1, along with the accepted terrestrial values from [7]. Oetliker et al. [8] derived solar wind Fe isotopic ratios using the Wind/MASS sensor. Their results have larger uncertainties but are in agreement with the present work. They obtained a value (in percent) of 8.5 (+0.5, -2.2) for Fe^{54}/Fe^{56} and an upper limit of 5% for Fe^{57}/Fe^{56}.

The Fe isotope ratios in Table 1 are, within the measurement uncertainties, consistent with no fractionation of Fe isotopes in the solar wind. They are however also consistent with a modest fractionation effect. A mass dependent isotopic fractionation has been reported for Ne, Mg and Si [9], with the heavier isotope depleted in the slow solar wind. The average magnitude of this effect

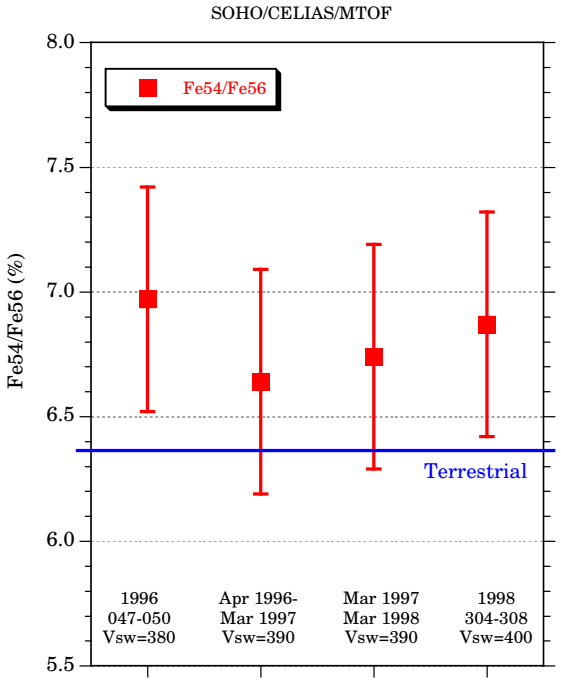

FIGURE 5. The derived ratios of Fe^{54} to Fe^{56} obtained during 4 distinct time intervals. The error bars denote 1-σ uncertainties and are dominated by systematic effects. The terrestrial value is indicated by the solid horizontal line.

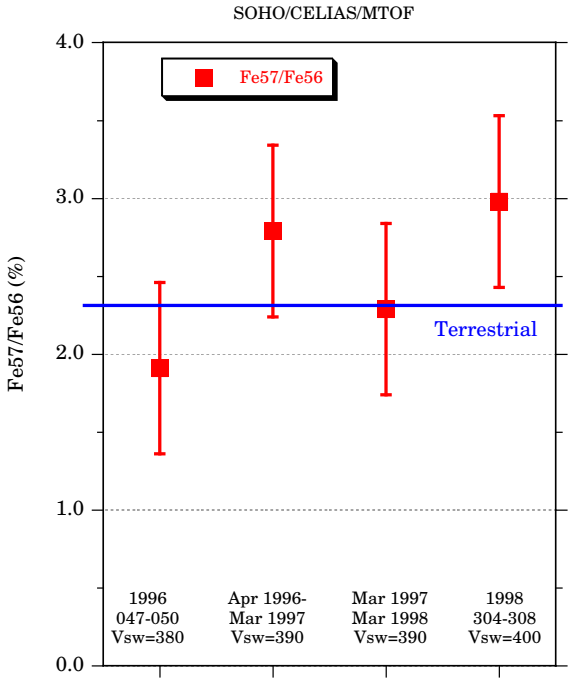

FIGURE 6. The derived ratios of Fe^{57} to Fe^{56} obtained during 4 distinct time intervals. The error bars denote 1-σ uncertainties. The terrestrial value is indicated by the solid horizontal line.

TABLE 1. Iron Isotopic Abundance Ratios

	Fe Isotopic Ratio (in percent)	
	This Work	Terrestrial*
Fe^{54}/Fe^{56}	6.8 ± 0.4	6.37
Fe^{57}/Fe^{56}	2.5 ± 0.5	2.31

* Beard and Johnson, 1999

was reported to be approximately 1.4% per amu. The Fe isotopic measurements reported here were all obtained from such slow solar wind flows. The fractionation effect from [9] would predict an enhancement of some 2.8% for Fe^{54}/Fe^{56} relative to the unfractionated solar composition, a result also consistent with our observed enhancement of about $(7 \pm 6)\%$ above the terrestrial value.

The current uncertainties in the isotope ratios presented in this paper are dominated by systematic effects. One such effect is the lack of knowledge of the precise shape of the TOF spectrum of Fe^{56} at TOF values that are far from the most probable value. We are attempting to improve our knowledge of the response in the wings of the TOF distribution by calibrating the MTOF spare instrument at an accelerator facility at the University of Bern [10]. The derived mass distribution can also be improved by carefully correcting for the effects caused by "electronic walk", in which different amplitude signals create slightly different times of flight. There is also a very small but statistically significant variation in the TOF with the residual ion energy (which can be determined from the MCP position measurement) and also with instrument temperature. We estimate that correcting for all of the above effects will decrease our uncertainty in the iron isotope ratios by perhaps a factor of two. It is also planned to examine the Fe isotope ratios in higher speed solar wind flows.

ACKNOWLEDGMENTS

We are grateful to all the individuals who participated in the design, the construction, and the calibration of CELIAS/MTOF. This research was supported by NASA grants NAG5-7678 and NAG5-9282.

REFERENCES

1. Anders, E., and Grevesse, N., *Geochimica et Cosmochimica Acta*, **53**, 197–214 (1989).
2. Bochsler, P., *Reviews of Geophysics*, **38**, 247–266 (1999).
3. Geiss, J., *Space Science reviews*, **85**, 241–252 (1998).

4. Hovestadt, D., Hilchenbach, M., Bürgi, A., Klecker, B., Laeverenz, P., Scholer, M., Grünwaldt, H., Axford, W. I., Livi, S., Marsch, E., Wilken, B., Winterhoff, H. P., Ipavich, F. M., Bedini, P., Coplan, M. A., Galvin, A. B., Gloeckler, G., Bochsler, P., Balsiger, H., Fischer, J., Geiss, J., Kallenbach, R., Wurz, P., Reiche, K.-U., Gliem, F., Judge, D. L., Ogawa, H. S., Hsieh, K. C., Möbius, E., Lee, M. A., Managadze, G. G., Verigin, M. I., and Neugebauer, M., *The SOHO Mission*, Kluwer Academic Publishers, Dordrecht, 1995, pp. 441–481.
5. Ipavich, F. M., Galvin, A. B., Lasley, S. E., Paquette, J. A., Hefti, S., Reiche, K.-U., Coplan, M. A., Gloeckler, G., Bochsler, P., Hovestadt, D., Grünwaldt, H., Hilchenbach, M., Gliem, F., Axford, W. I., Balsiger, A., Bürgi, A., Geiss, J., Hsieh, K. C., Kallenbach, R., Klecker, B., Lee, M. A., Managadze, G. G., Marsch, E., Möbius, E., Neugebauer, M., Scholer, M., Verigin, M. I., Wilken, B., and Wurz, P., *Journal of Geophysical Reasearch*, **103**, 17205–17213 (1998).
6. NAG, Numerical Algorithm Group, *NAG Fortran Library Manual, Mark 18*, NAG Ltd, Oxford, 1997, vol. 4, chap. E04.
7. Beard, B. L., and Johnson, C. M., *Geochimica et Cosmochimica Acta*, **63**, 1653–1660 (1999).
8. Oetliker, M., Hovestadt, D., Klecker, B., Collier, M. R., Gloeckler, G., Hamilton, D. C., Ipavich, F. M., Bochsler, P., and Managadze, G. G., *The Astrophysical Journal Letters*, **474**, L69–L72 (1997).
9. Kallenbach, R., Ipavich, F. M., Kucharek, H., Bochsler, P., Galvin, A. B., Geiss, J., Gliem, F., Gloeckler, G., Grünwaldt, H., Hefti, S., Hilchenbach, M., and Hovestadt, D., *Space Science Reviews*, **85**, 357–370 (1998).
10. Marti, A., Schletti, R., Wurz, P., and Bochsler, P., *Reviews of Scientific Instruments*, **72**, 1354–1360 (2001).